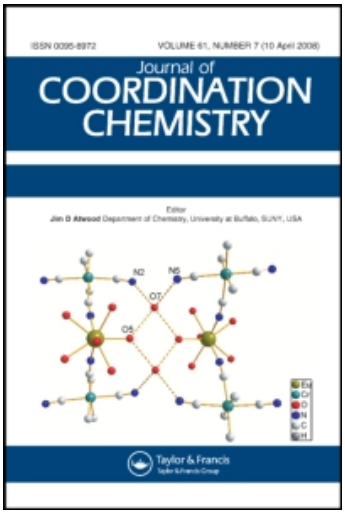

Journal of Coordination Chemistry
Publication details, including instructions for authors and subscription information:
http://www.informaworld.com/smpp/title~content=t713455674

Crystal structure and magnetic properties of tris(2-hydroxymethyl-4-oxo-4H-pyran- 5-olato-κ²O⁵,O⁴)iron(III)

K. Zaremba[a]; W. Lasocha[a]; A. Adamski[a]; J. Stanek[b]; A. Pattek-Janczyk[a]
[a] Faculty of Chemistry, Jagiellonian University, Kraków, Poland [b] Jagiellonian University, M. Smoluchowski Institute of Physics, Kraków, Poland

To cite this Article Zaremba, K. , Lasocha, W. , Adamski, A. , Stanek, J. and Pattek-Janczyk, A.(2007) 'Crystal structure and magnetic properties of tris(2-hydroxymethyl-4-oxo-4H-pyran- 5-olato-κ²O⁵,O⁴)iron(III)', Journal of Coordination Chemistry, 60: 14, 1537 — 1546
To link to this Article: DOI: 10.1080/00958970601084243
URL: http://dx.doi.org/10.1080/00958970601084243

Journal of Coordination Chemistry
Vol. 60, No. 14, 15 July 2007, 1537–1546

Taylor & Francis
Taylor & Francis Group

Crystal structure and magnetic properties of tris(2-hydroxymethyl-4-oxo-4H-pyran-5-olato-κ^2O^5,O^4)iron(III)

K. ZAREMBA†, W. LASOCHA†, A. ADAMSKI†,
J. STANEK‡ and A. PATTEK-JANCZYK*†

†Faculty of Chemistry, Jagiellonian University,
3 Ingardena Street, 30-060, Kraków, Poland
‡M. Smoluchowski Institute of Physics, Jagiellonian University,
3 Reymonta Street, 30-059, Kraków, Poland

(*Received 12 May 2006; in final form 1 July 2006*)

Tris(2-hydroxymethyl-4-oxo-4H-pyran-5-olato-κ^2O^5,O^4)iron(III) [Fe(ka)$_3$], has been characterised by magnetic susceptibility measurements Mössbauer and EPR spectroscopy. The crystal structure of [Fe(ka)$_3$] has been determined by powder X-ray diffraction analysis. Magnetic susceptibility and EPR measurements indicated a paramagnetic high-spin iron centre. Mössbauer spectra revealed the presence of magnetic hyperfine interactions that are temperature-independent down to 4.2 K. The interionic Fe^{3+} distance of 7.31 Å suggests spin-spin relaxation as the origin of these interactions.

Keywords: Fe(III) complexes; 4H-γ-Pyrones; *mer, fac* isomers; X-Ray powder diffraction; Structure; Magnetic susceptibility; Mössbauer spectroscopy

1. Introduction

Iron complexes of α-cycloketoenoles were patented by Hider *et al.* [1] as pharmaceuticals useful in the treatment of iron deficiency anaemia. In this connection, tris(maltolato)iron(III) was intensively investigated both *in vivo* and *in vitro* [2–5]. Its peculiar properties such as high solubility in water and stability in solution, non-charged character, low toxicity and rapid metabolism of ligands predisposed the complex to be a very promising remedy for certain types of anaemia. A ligand structurally related to maltol is kojic acid (Hka; 5-hydroxy-2-hydroxymethyl-4H-pyran-4-one). It is a hydroxypyrone of natural origin and possesses even more interesting properties than those mentioned above. Hka has been widely used in the food industry as an antioxidant, preventing food discoloration [6–8]. However, the most important applications of kojic acid are connected with its skin whitening ability [9, 10]. Additionally, a vanadyl complex of Hka exhibits insulin-mimetic features [11]. Kojic acid occurs naturally in many components of the human diet, and its complex with iron

*Corresponding author. Email: patjan@chemia.uj.edu.pl

ISSN 0095-8972 print/ISSN 1029-0389 online © 2007 Taylor & Francis
DOI: 10.1080/00958970601084243

may be considered as a potential iron-deficiency remedy. This is the reason why studies of this complex were mainly focused on properties in solutions such as solubility in various solvents [12] and stability [13]. Besides Maeda's work [14] on the insensitivity of $[Fe(ka)_3]$ to radiation in Mössbauer measurements, there are no papers describing the properties of $[Fe(ka)_3]$ in solid state in more detail.

This contribution initiates a series of efforts concerning the structures and properties of iron complexes of hydroxpyrones in the solid state. Kojic acid, structurally similar to the two hydroxypyrones maltol (3-hydroxy-2-methyl-4H-pyran-4-one) and ethylmaltol (3-hydroxy-2-ethyl-4H-pyran-4-one), exhibits different properties [12, 15, 16], among these being increased solubility due to the presence of the OH group in the aliphatic substituent of the pyran ring. The structures of iron complexes with maltol $[Fe(mal)_3]$ and ethylmaltol $[Fe(etmal)_3]$ were elucidated as *mer* [5] and *fac* [17] isomers, respectively. Odoko [17] suggested a *fac* configuration due to the bulky hydrophobic ethyl group in $[Fe(etmal)_3]$ in comparison to the methyl group in $[Fe(mal)_3]$. The structure of $[Fe(ka)_3]$ has not yet been solved. Considering the molecular structure of kojic acid (no substituent at α carbon in the pyran ring and the position of the CH_2OH group rather far from Fe–O bonds), the *mer* configuration in $[Fe(ka)_3]$ might be expected. The aim of present work was to investigate the structure and magnetic properties of $[Fe(ka)_3]$ studied by EPR and Mössbauer spectroscopy as well as magnetic susceptibility measurements.

2. Experimental

2.1. *$[Fe(ka)_3] \cdot 1/2H_2O$*

Chemicals were of analytical grade and used without further purification. $[Fe(ka)_3]$ was obtained by direct mixing of $Fe(ClO_4)_3 \cdot xH_2O$ and kojic acid in ethanol saturated with lithium carbonate [18]. The precipitate was recrystalised from ethanol, yielding very fine red crystals. The product composition was confirmed by elementary analysis and AAS. Anal. Calcd for $FeC_{18}H_{16}O_{12.5}$ (%): C, 44.3; H, 3.3; Fe, 11.4. Found: C, 44.4; H, 3.3; Fe, 11.0.

2.2. *X-ray structure analysis*

X-ray powder data were collected using a Philips X'PERT PW3710 diffractometer. Lattice parameters and the space group were determined using the PROSZKI package [19]. The structure was solved by global optimisation method using FOX [20]. The structure was completed and refined with a set of geometric constraints by the XRS–82 Rietveld program [21]. Details of the Rietveld analysis are presented in table 1 and the corresponding refinement plots are shown in figure 1. In the refinement procedure 85 restraints were used, 36 distances and 49 angles. Uniform weights were applied for bonds and angles. Weights for bonds were estimated assuming a tolerance equal to 0.02 Å, while angles were weighted by 0.6°. In final cycles of refinement, weight assigned to geometric restraints was about 20% of the diffraction data. Stronger geometric restraints caused an increase in R factors, while lower weights resulted in geometric instability. On the other hand, unrealistic distances in the central part of the

Table 1. Details of the Rietveld refinement of $[Fe(ka)_3] \cdot 1/2H_2O$.

Empirical formula	$C_{18}H_{16}FeO_{12.5}$
M	1480.16
2θ range, step size (°)	3.50–75.00, 0.2
Number of reflections	950
Number of observations	3475
Crystal system	Monoclinic
Space group	$C2/c$
a (Å)	26.771(8)
b (Å)	9.265(4)
c (Å)	19.308(6)
β (°)	126.43(2)
V (Å^3)	3853(1)
Z	8
T (K)	298
ρ (Calcd) (g cm^{-3})	1.68
Number of atoms	32
R_F (%)	14.7
R_{wp} (%)	12.3

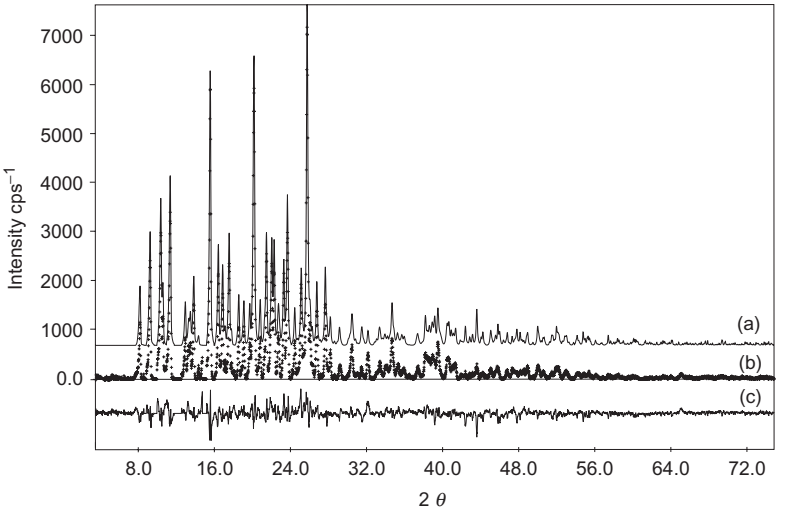

Figure 1. Rietveld refinement plots for $[Fe(ka)_3] \cdot 1/2H_2O$; (a) experimental pattern; (b) calculated profile; (c) difference profile.

molecule were obtained when stronger restraints for side groups were assumed. Applied texture correction was based on the formula $I' = I\exp(G\cos\alpha)$, where texture direction and G coefficient, describing strength of texture, are [001] and −0.38, respectively. Crystallographic data for the structure analysis have been deposited at the Cambridge Crystallographic Data Centre with deposition number CCDC 278114.

2.3. *Physical methods*

Magnetic measurements (powdered samples) were carried out with a Quantum Design SQUID MPMS–XL5 magnetometer. Magnetization was measured at a constant

magnetic field of 5 T in the temperature range 2–293 K and in a variable magnetic field (0–5 T) at a constant temperature of 2 K. CW-EPR X–band spectra were recorded at ambient and liquid nitrogen (77 K) temperatures with a Bruker ELEXSYS E–500 spectrometer operating at a 100 kHz field modulation. EPR parameters were evaluated by using the SIM32 simulation program [22]. Mössbauer spectra were recorded using a conventional spectrometer in transmission geometry with a ^{57}Co/Rh source. Samples were prepared in pellets with a thickness of ca 10 mg Fe cm^{-2}. Measurements were carried out at 298, 80, 26 and 4.2 K. Spectra were numerically analysed using the Voigt-based fitting method of Rancourt and Ping for hyperfine field distributions (HFD) [23]. The full width at half maximum (FWHM) was fixed at 0.24 mm s^{-1}. Isomer shift values are quoted relative to α-Fe.

3. Results and discussion

3.1. *Structural data*

[Fe(ka)$_3$] crystallizes in the monoclinic space group $C2/c$. In the difference Fourier map one water molecule was found in the 4c position (O32 in table 2). The unit cell of [Fe(ka)$_3$], depicted in figure 2, contains four water molecules per eight molecules of complex, confirming stoichiometry of [Fe(ka)$_3$]$\cdot 1/2H_2O$. A complete list of atomic coordinates and isotropic temperature factors is presented in table 2. The temperature factors have the form of $\exp(-8\pi^2 U(\sin\theta/\lambda)^2)$, but the temperature factors found by powder methods are not particularly precise.

The molecular structures of iron(III) complexes with ethylmaltol and maltol, previously determined from single crystal data by direct methods, can be described as comprising three bidentate ligands forming a distorted octahedral environment in a *mer* configuration in the case of [Fe(mal)$_3$] [5] and a *fac* configuration in the case of [Fe(etmal)3] [17]. Similarly, a distorted octahedral coordination sphere was observed in the molecular structure of [Fe(ka)$_3$] (figure 3). Two kinds of Fe–O bonds can be distinguished in this molecule (table 3), shorter Fe–O_{OH} and longer Fe–$O_{C=O}$; the $O_{OH-Fe-OC=O}$ angles also deviate from 90°. [Fe(ka)$_3$] adopts the *fac* configuration, in contrast earlier suggestions [17]. Thus the isomer obtained is influenced by intermolecular interactions, rather than by the substituent at the $C2$ position in the pyran ring alone.

3.2. *Magnetic and spectroscopic properties*

The results of magnetic measurements are shown in figures 4 and 5. The temperature dependence of the magnetic susceptibility of [Fe(ka)$_3$] reveals changes of χT from 4.69 cm^3 K mol^{-1} at ambient temperatures to 4.24 cm^3 K mol^{-1} at 14 K, and 3.60 cm^3 K mol^{-1} at 2 K. The data conform to the Curie–Weiss law with $C = 4.321(4)$ cm^3 K mol^{-1} and $\theta = -0.37$ K. The expected C value for the iron(III) ion with $g = 2.0$ and $S = 5/2$ is 4.375 cm^3 K mol^{-1}. The small difference in the calculated C constant (1.2%) may be explained by assuming either very weak spin-orbital coupling or the presence of antiferromagnetic interactions. Measurements performed at constant temperature and variable magnetic field (figure 5) are in agreement with

Table 2. List of atomic coordinates and isotropic temperature factors for $Fe(ka)_3] \cdot 1/2H_2O$.

	x	*y*	*z*	*U*
Fe1	0.3471(8)	0.887(2)	0.936(1)	0.120(11)
O7	0.363(2)	1.199(6)	0.728(2)	0.13(2)
C8	0.426(2)	1.164(5)	0.779(3)	0.13(3)
O2	0.425(1)	0.933(4)	0.935(3)	0.13(2)
C3	0.409(1)	1.026(6)	0.874(3)	0.13(3)
C4	0.344(2)	1.065(7)	0.817(4)	0.13(3)
O5	0.305(1)	1.029(5)	0.837(3)	0.13(2)
C6	0.326(2)	1.166(6)	0.754(4)	0.13(3)
C9	0.451(2)	1.063(8)	0.852(3)	0.13(3)
O10	0.329(2)	0.695(4)	0.868(2)	0.02(1)
C11	0.374(2)	0.593(4)	0.921(2)	0.02(2)
C12	0.418(2)	0.624(3)	1.012(2)	0.02(2)
O13	0.407(2)	0.737(4)	1.041(2)	0.02(2)
C14	0.457(3)	0.512(4)	1.070(2)	0.02(2)
C15	0.457(2)	0.377(3)	1.036(2)	0.02(2)
O16	0.417(2)	0.353(4)	0.946(2)	0.02(1)
C17	0.371(2)	0.457(5)	0.891(2)	0.02(2)
O18	0.370(1)	1.055(4)	1.024(2)	0.05(1)
C19	0.328(2)	1.070(5)	1.034(3)	0.05(2)
C20	0.275(2)	0.968(5)	0.991(4)	0.05(2)
O21	0.277(2)	0.855(3)	0.948(3)	0.05(1)
C22	0.231(2)	0.967(8)	1.013(5)	0.05(2)
O23	0.235(2)	1.085(6)	1.068(4)	0.05(1)
C24	0.291(3)	1.169(8)	1.116(5)	0.05(2)
C25	0.340(2)	1.152(7)	1.105(4)	0.05(2)
C26	0.460(3)	1.271(7)	0.759(5)	0.19(5)
O27	0.409(3)	1.395(6)	0.703(4)	0.19(3)
C28	0.486(4)	0.235(3)	1.082(3)	0.03(2)
O29	0.527(2)	0.259(5)	1.171(3)	0.03(1)
C30	0.294(4)	1.255(10)	1.189(7)	0.07(2)
O31	0.337(2)	1.385(6)	1.205(4)	0.07(2)
O32	0.000	−0.35(1)	0.25	0.38(13)

this interpretation. A lack of any hysteresis confirms the paramagnetic character of the complex. The calculated value of the magnetic moment μ_o (extrapolated to infinity) equals 4.73(2) μB and is also slightly lower than the value of 5 μB expected for $g = 2.0$ and $S = 5/2$ iron(III). Distorted octahedral coordination of iron as well as the high-spin state is confirmed independently by EPR spectroscopy technique. The high-spin configuration is characteristic of a weak ligand field. All EPR spectra can be described by the effective spin Hamiltonian $H = g\beta\mathbf{HS} + D[S_z^2 - 1/3S(S+1)] + E[S_x^2 - S_y^2]$ with $S = 5/2$, where D and E are the parameters of the zero-field splitting (ZFS), characterising, respectively, the axial and rhombic parts of distortion of the crystal field from octahedral symmetry; the other symbols have their usual meanings [24, 25]. EPR spectrum (see figure 6) recorded for $[Fe(ka)_3]$ at ambient temperature is similar in shape to that obtained at liquid nitrogen temperature. In both cases, the line is distinctly broadened ($\Delta H_{pp} \approx 1000$ G), making detailed analysis difficult. The low-temperature spectrum of $[Fe(ka)_3]$ exhibits a broad maximum at $g \approx 5.0$ and a weaker one at $g \approx 2.0$–2.4. There is no fine structure resolved in any spectrum. The g factor values equal to 5.0 and 2.0 are close to those usually ascribed to $g_\perp$ and $g_\parallel$ of high-spin Fe^{3+} in a distorted octahedral environment [24, 26]. In the present case $g_\perp$ is higher than 4.3, explained by a deviation of the E/D ratio from 1/3 [24]. This is not surprising, if one

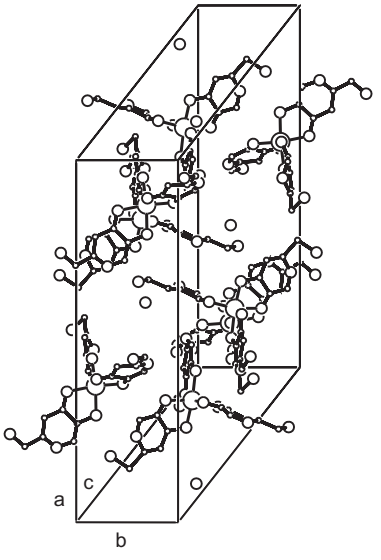

Figure 2. Packing of molecules in the unit cell of $[Fe(ka)_3] \cdot 1/2H_2O$; large circles denote Fe, medium circles O, and small circles C atoms.

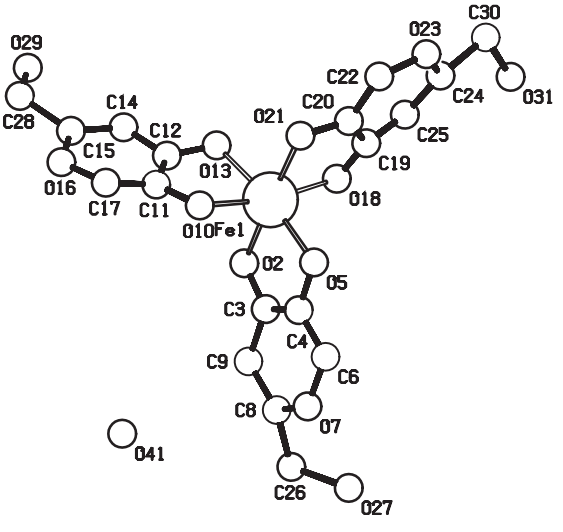

Figure 3. The structure of $[Fe(ka)_3]$.

Table 3. Fe–O bond lengths (Å) in $Fe(ka)_3] \cdot 1/2H_2O$.

Fe1–O2	2.14(0.05)
Fe1–O5	2.02(0.05)
Fe1–O10	2.09(0.04)
Fe1–O13	2.18(0.05)
Fe1–O18	2.11(0.04)
Fe1–O21	2.04(0.07)

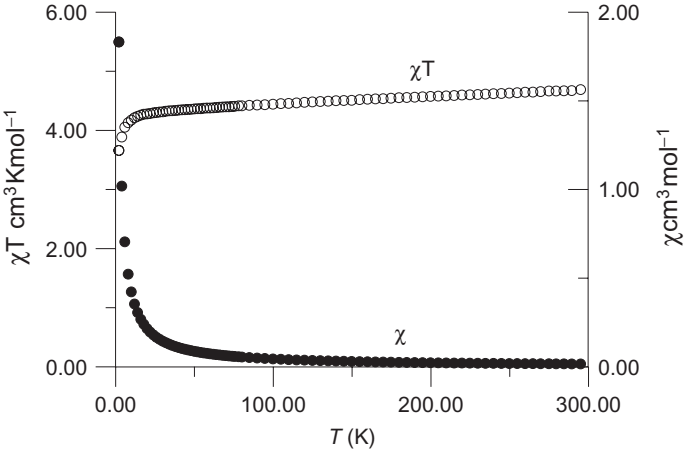

Figure 4. Dependence of χ and χT on temperature.

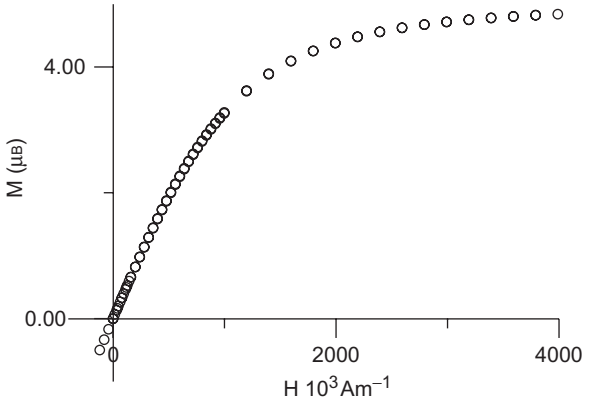

Figure 5. Dependence of magnetization on magnetic field H.

takes into account the fact that the D value is expected to be small for Fe(III) ions stabilized in a symmetry close to octahedral [27]. The presence of the broad signal appearing at $g \approx 2.3$ in the spectrum of $[Fe(ka)_3]$ at ambient temperature, which is absent at 77 K, indicates the tendency of this system to undergo relaxation processes.

Mössbauer spectra of $[Fe(ka)_3]$ (figure 7) have the rather atypical shape of an asymmetric doublet with non-Lorenzian line shape. The wide velocity range (–2.5 to $+3\,mm\,s^{-1}$) of the resonant absorption is evidence for magnetic hyperfine interactions and the asymmetry of the spectra indicates quadrupole interactions. In magnetically ordered materials a static effective magnetic field acting on the nucleus results in nuclear Zeeman splitting, and the spectrum reveals the hyperfine structure. In paramagnetic materials, especially in biological or organic samples where relaxation processes are slow, magnetic interactions are also possible to observe. In such cases the concept of effective magnetic field is useless and should be replaced by a more complex approach.

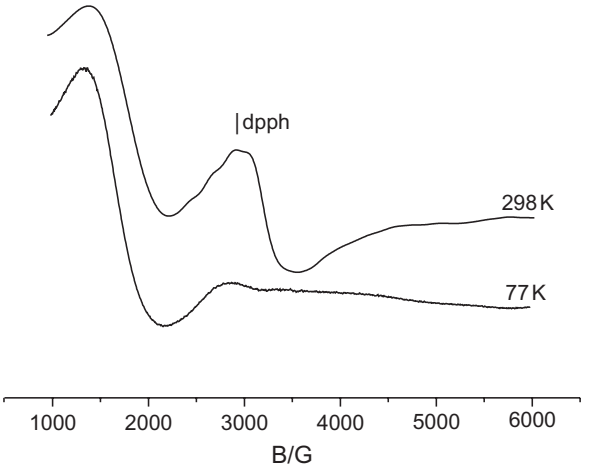

Figure 6. EPR spectra of $[Fe(ka)_3]\cdot 1/2H_2O$ recorded at 298 and 77 K.

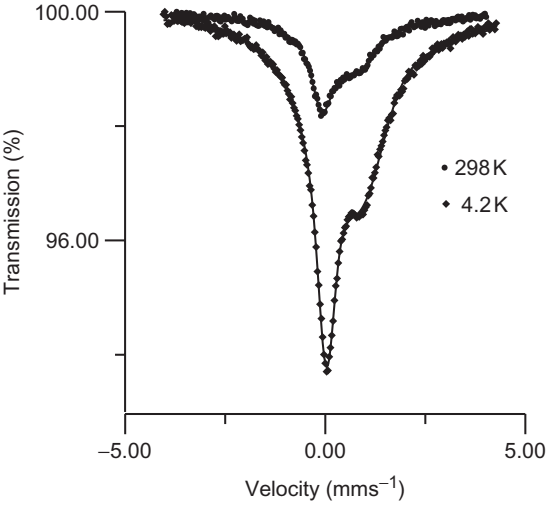

Figure 7. Mössbauer spectra of $[Fe(ka)_3]\cdot 1/2H_2O$ recorded at 298 and 4.2 K.

To include the hyperfine interactions it is necessary to add two terms to the Hamiltonian above, $\boldsymbol{I}\mathbf{P}\boldsymbol{I}$ and $\boldsymbol{I}\mathbf{A}\boldsymbol{S}'$, to give $H = g\beta\mathbf{H}\mathbf{S} + D[S_z^2 - 1/3S(S+1)] + E[S_x^2 - S_y^2] + \boldsymbol{I}\mathbf{P}\boldsymbol{I} + \boldsymbol{I}\mathbf{A}\boldsymbol{S}'$, representing quadrupole and magnetic hyperfine interactions at the nucleus. The ^{6}S state of Fe(III) splits into three Kramers doublets, $\pm 1/2$, $\pm 3/2$, $\pm 5/2$ with effective spin $S' = 1/2$. In the general case, the non-axial tensor $\mathbf{A}$ leads to $(2S'+1)^2(2I_g+1)(2I_e+1) = 32$ nuclear transitions for each Kramers doublet. In principle it is possible to simulate the spectra by knowing the exact values of D, E and $\mathbf{A}$, but any attempt to obtain these parameters by a fitting procedure from a measured spectrum is hopeless. Magnetic hyperfine interactions may be additionally

Table 4. Mössbauer parameters for $Fe(ka)_3] \cdot 1/2H_2O$.

T (K)	IS (mms^{-1})	QS (mms^{-1})	$H_{average}$ (T)	σH (T)
4.2	0.51	0.59	5.6	6.9
26	0.50	0.53	5.9	7.3
80	0.49	0.49	5.6	7.0
300	0.35	0.43	5.1	6.4

complicated by relaxation processes, i.e., transitions between Kramers doublets. These lead to the time-dependent Hamiltonian. In such situations the only way to reproduce the experimental spectra is to fit them by a gaussian distribution of the effective magnetic field (HFD) [28] (table 4).

The obtained isomer shift and quadrupole splitting values are characteristic of high-spin Fe^{3+} ions. For such ions the electric field gradient originates mainly from lattice contributions. In the present case the lattice contribution arises both, from different negative charges localised on oxygen O_{OH} and $O_{C=O}$ atoms and from the asymmetric ligand arrangement. The lack of significant changes of average hyperfine field H and its distribution with temperature decrease may suggest relaxation processes of the spin-spin mechanism. In fact, the distances between iron ions in $[Fe(ka)_3]$ (7.31°A) are comparable to distances found in bidentate iron complexes (Fe–Fe = 6.56 Å in lithium trisoxalatoferrate(III) pentahydrate [30] and 6.86 Å in sodium trismalonatoferrate(III) octahydrate [29]) where spin-spin relaxation phenomena were also suggested. It is interesting to note that the shape of the spectra may be reproduced in general by a simplified Blume–Tjone relaxation model [31, 32].

Acknowledgements

The authors are grateful to Prof. K. Tomala (M. Smoluchowski Institute of Physics, Jagiellonian University, Kraków, Poland) for magnetic measurements and to Dr J. Żukrowski (AGH University of Science and Technology, Kraków, Poland) for recording the Mössbauer spectra at 26 and 4.2 K.

References

[1] R.C. Hider, G. Kontioghiorges, J. Silver, M.A. Stockham. *Appl. Eur. Pat. Appl.*, EP107, **2 May**, 458 (1984).
[2] D.M. Reffitt, T.J. Burden, P.T. Seed, J. Wood, R.P.H. Thompson, J. Powell. *Ann. Clin. Biochem.*, **37**, 457 (2000).
[3] M.A. Stockham. *PCT Int. Appl.*, WO 2003097627 A1, 27 Nov 2003, 45.
[4] M. Uher, M. Chalabala, J. Cizmarik. *Ceska a Slovenska Farmacie*, **49**, 288 (2000).
[5] M.T. Ahmet, C.S. Frampton, J. Silver. *J. Chem. Soc., Dalton Trans.*, **5**, 1159 (1988).
[6] O.K. Lee, K. Sob, D. Hee, Y.S. Jang, S.J. Moon, Y.C. Shim, Y.H. Lee, D.S. Park, H.K. Kim, H.K. Kang, H.S. Baek, J.S. Hwang. *PCT Int. Appl.*, WO 2002083092 A1 24 Oct 2002, 25.
[7] I. Hansenne, A. Galdi, H. Fares, S.P. Foltis. *U.S. Pat. Appl. Publ.*, US 2004028642 A1 12 Feb 2004, 12.
[8] J. Creeth, K. Molloy, P. Wright. *PCT Int. Appl.*, WO 2000016736 A1, 30 Mar 2000, 19.

[9] G.J. Nohynek, D. Kirkland, D. Marzin, H. Toutain, C. Leclerc-Ribaud, H. Jinnai. *Food Chem. Toxicol.*, **42**, 93 (2004).
[10] I.A. Topol, S.K. Burt, A.A. Rashin, J.W. Erickson. *J. Phys. Chem. A.*, **104**, 866 (2000).
[11] V.G. Yuen, P. Caravan, L. Gelmini, N. Glover, J.H. McNeill, I.A. Setyawati, Y. Zhou, C. Orvig. *J. Inorg. Biochem.*, **68**, 109 (1997).
[12] J. Burgess, C.D. Hubbard, M.S. Patel. *Trans. Metal Chem.*, **27**, 134 (2002).
[13] J. Makáová. *Coord. Chem. Rev.*, **160**, 161 (1997).
[14] Y. Maeda, T. Katsuki, Y. Morinaga, Y. Takashima. *Bull. Chem. Soc. Jpn*, **54**, 2662 (1981).
[15] W.A.E. McBryde, G.F. Atkinson. *Can. J. Chem.*, **39**, 510 (1961).
[16] (a) Z.-S. Lu, J. Burgess, R. Lane. *Trans. Metal Chem.*, **27**, 239 (2002); (b) M.T. Ahmet, C.S. Frampton, J. Silver. *J. Chem. Soc., Dalton Trans.*, 1159 (1988).
[17] M. Odoko, K. Yamamoto, M. Hosen, N. Okabe. *Acta Cryst.*, **C59**, 121 (2003).
[18] A. Pattek-Janczyk, K. Zaremba, J. Stanek, A. Adamski. *Ann. Pol. Chem. Soc.*, **3**, 280 (2004).
[19] W. Lasocha, K. Lewinski. *J. Appl. Cryst.*, **27**, 437 (1994).
[20] V. Favre-Nicolin, R. Cerny. *J. Appl. Cryst.*, **35**, 734 (2002).
[21] C. Baerlocher, A. Hepp, L.B. McCusker. *XRS-82: The X-Ray Rietveld System of Crystallographic Programs for Powder Data*, University of Zurich, Zurich (1982).
[22] T. Spalek, P. Pietrzyk, Z. Sojka. *J. Chem. Inf. Model.*, **45**, 18 (2005).
[23] D.G. Rancourt, J.Y. Ping. *Nucl. Instrum. Meth. Phys. Res. B.*, **58**, 85 (1991).
[24] R. Kirmse, J. Stach. *Spektroskopia EPR, Zastosowanie w chemii*, Jagiellonian University Press, Kraków (1994).
[25] X. Hu, K. Meyer. *Inorg. Chim. Acta*, **337**, 53 (2002).
[26] H. Levanon, G. Stein, Z. Luz. *J. Am. Chem. Soc.*, **90**, 5292 (1968).
[27] (a) J.R. Pilbrow. *Mol. Phys.*, **50**, 841 (1983); (b) J.R. Pilbrow. *Transition Ion Electron Paramagnetic Resonance*, Clarendon Press, Oxford (1990).
[28] D.G. Rancourt. *Mosmod Mössbauer Analysis Sofware*, Module 9.2. (1996).
[29] S. Calogero, L. Stievano, L. Diamandescu, D. Mihil-Trbsanu, G. Valle. *Polyhedron*, **16**, 3953 (1997).
[30] J.P. Declercq, J. Feneau-Dupont, J. Ladriere. *Polyhedron*, **14**, 1943 (1995).
[31] M. Blume. *Phys. Rev. Lett.*, **14**, 96 (1965).
[32] M. Blume. *Phys. Rev. Lett.*, **18**, 305 (1967).